# Advanced Modeling of Charge Trapping: RTN, 1/f noise, SILC, and BTI

(Invited Paper)

W. Goes*, M. Waltl*, Y. Wimmer†, G. Rzepa*, and T. Grasser*
*Institute for Microelectronics, TU Wien, Vienna, Austria
†Christian-Doppler Laborartory for TCAD

***Abstract*—In the course of years, several models have been put forward to explain noise phenomena, bias temperature instability (BTI), and gate leakage currents amongst other reliability issues. Mostly, these models have been developed independently and without considering that they may be caused by the same physical phenomenon. However, new experimental techniques have emerged, which are capable of studying these reliability issue on a microscopic level. One of them is the time-dependent defect spectroscopy (TDDS). Its intensive use has led to several interesting findings, including the fact that the recoverable component of BTI is due to reaction-limited processes. As a consequence, a quite detailed picture of the processes governing BTI has emerged. Interestingly, this picture has also been found to match the observations made for other reliability issues, such as random telegraph noise, 1/f noise, as well as gate leakage currents. Furthermore, the findings based on TDDS have lead to the development of capture/emission time (CET) maps, which can be used to understand the dynamic response of the defects given their widely distributed parameters.**

## Introduction

In order to improve on the device performance, large technological efforts have been made to scale down the transistor geometries to present-day dimensions. Despite the achieved progress, old unresolved reliability problems, such as BTI [1] and random telegraph noise (RTN) [2], have remained or become worse. In the case of RTN, the threshold voltage ($V_{\mathrm{th}}$) may have fluctuations larger than typically used lifetime criteria of e.g. $30\,\mathrm{mV}$. These fluctuations are the result of charge capture or emission events into and out of oxide defects [2]. Interestingly, each defect produces fluctuations with its own characteristic step height and time constants — a fact that has been exploited to identify the contributions of single defects in RTN signals. However, RTN experiments can only monitor the behavior of a defect around a certain gate bias and therefore suffer from a quite narrow experimental window. This is in contrast to the recently introduced TDDS method, which is used to analyze the recoverable component of BTI degradation on small-area devices. It covers the wide spectrum of non-equilibrium conditions, encountered for the stress conditions in BTI experiments. Due to this advantage, this method has proven extremely useful for studying the gate bias and temperature dependences of the charge capture ($\tau_{\mathrm{c}}$) and emission ($\tau_{\mathrm{e}}$) times. Since it allows to study single defects, it provides direct insight into the mechanism behind charge capture and emission.

## TDDS and Its Implications

During a TDDS experiment, the gate bias is switched between the stress and recovery level, thereby initiating a certain kind of reactions, such as the charging and discharging of defects in the dielectric. These reactions are traced in the drain current based on their step heights and time constants. As they are stochastic processes, the bias switches must be repeated hundreds of times for accurate determination of their corresponding time constants, such as the mean capture ($\tau_{\mathrm{c}}$) and emission ($\tau_{\mathrm{e}}$) times in the case of charge trapping. An in-depth statistical analysis [3] revealed that charge capture and emission follow a Poisson process, characterized by its exponential probability density functions. Such a process is the result of a first-order reaction, such as elastic tunneling of charge carriers, pure thermal transitions (any kind of an atomic rearrangement without a charge transfer), and nonradiative multiphonon (NMP) transitions [4, 5]. All of them are possibly involved in charge trapping but the concept of the traditional reaction-diffusion model must be ruled out since it is incompatible with a Poisson process.

Beside these physical aspects, TDDS has also revealed several features which all investigated BTI defects have in common:

(*i*) Charge capture as well as emission are temperature dependent and have an activation energy in the range of $0.4 - 1.5\,\mathrm{eV}$ [6].

(*ii*) Two defect types exist, which significantly differ in their bias dependence. As demonstrated in Fig. 1, the emission times of the "fixed oxide traps" are insensitive to the gate bias while those of the "switching oxide traps" show a drop at lower voltages [7].

(*iii*) Charge capture is strongly accelerated with increasing gate bias, but slowed down with higher frequencies in AC stress experiments [8, 9].

(*iv*) Defects in their neutral charge state were found to disappear for random amounts of time, during which they do not capture or emit charge carriers. This volatility is thermally activated and has been tentatively linked to hydrogen in the dielectric [10].

(*v*) The capture and emission times extracted from RTN and TDDS measurements match well (for instance shown for the defect B3 in Fig. 1). As this agreement is found for a large majority of the investigated defects, we conclude that BTI and RTN are dominated by the same defects (cf. Fig. 2) and must therefore be investigated together [11].

(*vi*) TDDS studies on SiON nMOSFETs have revealed that *electron* capture and emission exhibit similar gate bias and temperature dependences as the fixed and switching hole traps in pMOSFETs. Interestingly, the same trapping behavior was also observed in device technologies based on high-$\kappa$ dielectrics [12]. This suggests that charge trapping in these cases rests upon the same general concepts with similar physical processes being involved [13].

978-1-4799-5288-5/14/$31.00 

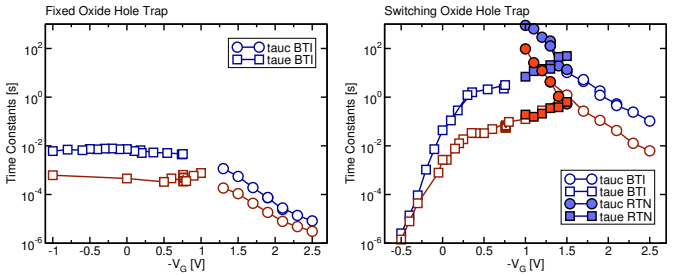


Fig. 1: Hole capture and emission times measured by TDDS (open symbols) and RTN (filled symbols) measurements. Two distinct kinds of defects are observed, which feature markedly different gate bias dependences. The exemplaric traps B1 (left) and B3 (right) are shown as representatives for the "fixed oxide trap" and the "switching oxide trap", respectively. Furthermore, it is emphasized that the time constants extracted from TDDS and RTN measurements match excellently, indicating that BTI and RTN are two faces of the same coin.

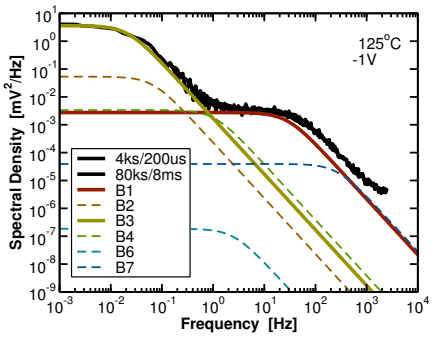


Fig. 2: The power spectral densities extracted from noise measurements (black symbols) is well explained by the contributions of single BTI defects extracted by TDDS (lines), indicating that BTI and RTN are caused by the same defects.

The above observations result in a quite restrictive set of criteria for any reliability model that should cover the recoverable component of BTI as well as RTN. The simplest and most natural approach would be a two-state model, in which the forward and the backward transition between the two charge states are described by NMP processes. The underlying NMP theory [4, 14, 15] accounts for the contribution of lattice vibrations which ultimately allow the charge trapping processes as explained in the configuration coordinate diagram of Fig. 3. The NMP processes in a two-state model predict a pronounced temperature activation as well as a strong gate bias dependence for the capture and emission times. However, this model can neither give an explanation for the measured frequency dependence in the capture times nor reproduce the constant emission times over a large gate bias range of more than 1 V. The latter observation is reminiscent of pure thermal transitions, which are to first order independent of the gate bias. Such transitions would occur in bistable defects, which have two meta-/stable configurations separated by a thermal barrier. Interestingly, bistable defects, such as the $E'$ center in the Harry-Diamond-Laboratory model [16], have already been proposed in the context of device reliability. Motivated by this idea, the defect model was extended to a bistable defect but with four states as in the state diagram of Fig. 4. In this model, charge capture and emission are now two-step processes between the stable states 1 and 2. Both can be reached via either of the metastable states $1'$ or $2'$, which opens two pathways for capture and emission. While one pathway

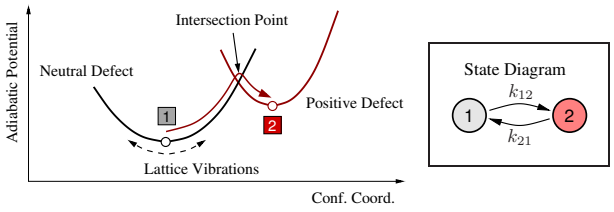


Fig. 3: **Left**: Configuration coordinate diagram for hole capture. The defect in its neutral (1) and positive (2) charge state is represented by the black and red adiabatic potential energy surfaces. In the harmonic approximation, these surfaces assume a parabolic shape for small atomic displacements. In the classical limit of the NMP theory, a transition can only take place at the intersection point of the two parabolas. Therefore, the neutral defect has to be thermally excited up to the intersection point via lattice vibrations. There, the actual tunneling process of the charge carrier may occur and the positive defect can further relax to its new equilibrium configuration. It is noted that the relative energetic positions of the two parabolas vary with the oxide field, giving rise to a strong gate bias dependence. **Right**: State diagram of the two-state model with a neutral (gray circle) and positive (red circle) charge state. The transition rates $k_{12}$ and $k_{21}$ are described by the NMP theory.

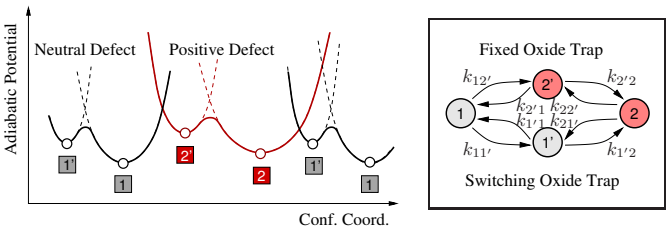


Fig. 4: **Left**: State diagram of the four-state NMP model. The defect is present in a neutral (1) and a positive (2) charge state, where each of them has a second metastable state marked by a prime ($1'$,$2'$). The NMP transitions $1 \leftrightarrow 2'$ and $1' \leftrightarrow 2$ occur between different charge states. The thermal transitions $1 \leftrightarrow 1'$ and $2 \leftrightarrow 2'$ only involve same charge states. The latter transitions are associated with a structural rearrangement of the defect and are modeled using Arrhenius-type expressions. The adiabatic potentials determine the defect parameters, such as the thermodynamic trap level $E_{\mathrm{T}}$, which can be calculated as the energy difference between the states 1 and 2. The shape of the adiabatic potentials varies from defect to defect and therefore gives rise to distributed defect parameters, which determine the trapping behavior of the defects. **Right**: State diagram of the four-state NMP model. Regarding hole emission, the two pathways from state 2 to 1 can explain the different gate bias behavior of fixed and switching oxide traps.

$(2 \leftrightarrow 1' \rightarrow 1)$ is associated with the switching trap behavior, the other $(2 \leftrightarrow 2' \rightarrow 1)$ can explain the fixed oxide traps (see Fig. 5). Interestingly, the four-state NMP model was also found to reproduce the frequency dependence in item (*iii*), as demonstrated in [8]. As such, this model gives a detailed description of the recoverable BTI degradation.

In contrast to the recoverable component of BTI, much less is known about the permanent component. In the two-stage model [18], it is assumed to be coupled to the charge trapping process while in [1, 6] it is modeled as a separate and independent process. In order to account for the permanent BTI degradation, the four-state NMP model can also be extended within the framework of the two-stage model [18]. There, a positive defect is allowed to undergo a defect transformation to a new state with a fixed positive charge. However, the four-state NMP model cannot account for the volatility of the defects, mentioned in item (*iv*). Consequently, the model has to include an additional inactive state labeled 0, in which the

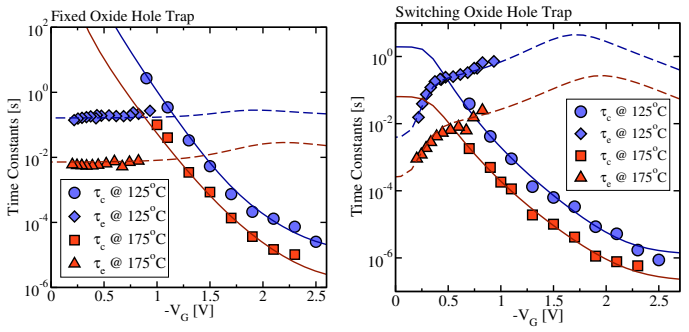


Fig. 5: Comparison of the simulated capture (solid lines) and emission (dashed lines) times with the TDDS data (symbols) for the fixed (left) and the switching (right) oxide hole traps. In the simulations, we employed the classical high-temperature limit of the NMP theory [17], which provides a good approximation at usual device operation temperatures. It is shown that the four-state NMP model nicely reproduces the essential features observed in TDDS experiments.

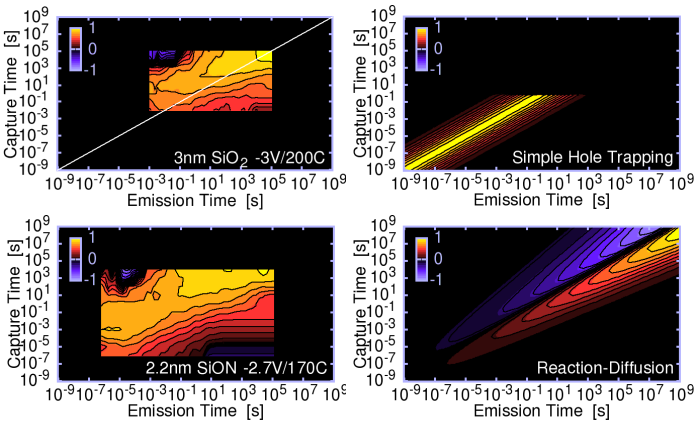


Fig. 6: The experimental CET maps (left) of a $SiO_2$ and a SiON device show a wide distribution of capture and emission times, indicating wide distributions of trap parameters. A simple hole trapping model and the reaction diffusion model (both right) yield CET maps which markedly differ from the experimental ones, and therefore cannot explain BTI.

defect cannot capture a charge carrier. As the defects probably vanish in their neutral charge state [19], the state 0 must be connected to either of the states 1 or $1'$. The exact chemical reaction behind the transition $0 \leftrightarrow 1/1'$ has not been clarified yet. However, it is likely to involve hydrogen since the amount of volatility in the recoverable BTI defects was found to vary with the background hydrogen content in the dielectric. This suggests that possible defect candidates are likely to contain hydrogen atoms, as is for instance the hydrogen bridge [20, 21].

## Capture/Emission Time Maps

The four-state NMP model includes metastable states, which are only passed temporarily during a capture or emission event. For DC stress conditions, it can be reduced to an effective two-state model, essentially showing the behavior of first-order reactions [8, 22]. As a consequence, the BTI degradation and recovery curves of large-area devices can be interpreted as a collection of "independent" first-order processes with certain combinations of capture and emission times for each defect. As such, one can build capture/emission time (CET) maps, in which each defect contributes with a certain threshold voltage shift. These CET maps (see Fig. 6 can be calculated from a complete set of BTI recovery curves, which include all combinations of stress and relaxation times within a typical measurement window.

Experimental CET maps [8, 23, 24] were found to show wide distributions of capture and emission times ranging from microseconds up to at least 10 ks and have their strongest contributions somewhere close to the diagonal $\tau_c = \tau_e$. Analytically, they have been successfully described by a combination of two bivariate Gaussian distributions, corresponding to the recoverable and the permanent component of BTI, respectively. It is noted here that the capture and emission times are directly related to the defect parameters of the four-state NMP model. As such, the observed distributions of capture and emission times reflect a wide spread in the defect parameters. The latter can be argued to be due to large variations of bond lengths and angles in the atomic structures of the defects, consistent with theoretical investigations [25–27]. Interestingly, it could also be demonstrated that the reaction-diffusion model [28] as

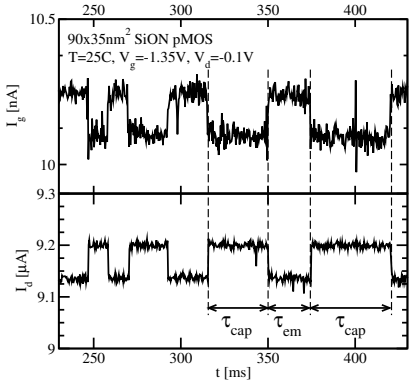


Fig. 7: Simultaneously recorded $I_g$ (upper panel) and $I_d$ traces (lower panel) [29]. Upon the hole capture (after a time period of $\tau_c$), the charged defect reduces $I_d$ and at the same time a significant increase in $I_g$ is observed.

well as elastic tunneling of charge carriers yield CET maps which are distinct from the experimental ones. Therefore both models must be ruled out as a possible explanation for BTI (cf. Fig. 6).

## The Four-State NMP Model as an Explanation for Stress-Induced Leakage Currents

Recent investigations [29–32] have revealed that the fluctuations in the drain and the gate current can be correlated (see Fig. 7). It may be argued that this correlation is associated with the captured charge which locally repels the inversion layer thereby decreasing the direct tunneling current. However, simulations based on the non-equilibrium Green's function method have demonstrated that this effect can be ruled out due to a too small magnitude of the gate current fluctuations [33]. Another explanation [34, 35] is based on a four-state NMP model and relies on trap-assisted tunneling (TAT) [36–38] through the defect producing the drain current noise. As illustrated in Fig. 8, the TAT current is described by two consecutive NMP transitions $1'_s \leftrightarrow 2 \leftrightarrow 1'_p$. It is emphasized that this current only flows upon hole capture when the defect is positive (state 2) but is stopped upon hole emission when

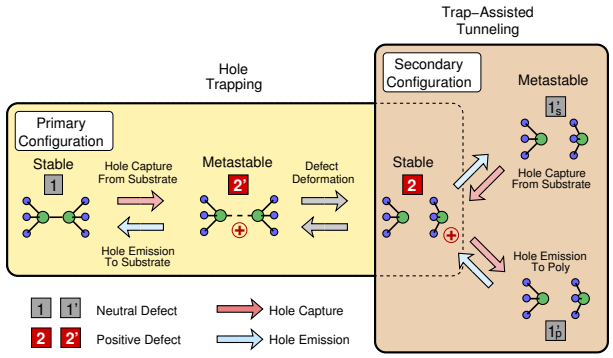


Fig. 8: Refined state diagram of the multi-state defect model explained using the oxygen vacancy as an example. Hole capture and emission still occur via transitions between the states 1 and 2 over the metastable state 2′. However, the state 1′ has to be split in order to differentiate whether the hole is located in the substrate (s) or the poly-gate (p). With this modification in the state diagram, one can define a TAT process in which the hole is transferred from the substrate into the poly-gate and can therefore contribute to a gate current.

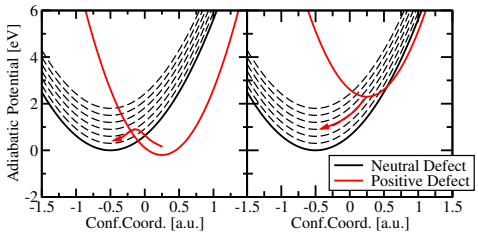


Fig. 9: Configuration coordinate diagram for hole emission in the strong (left) and weak (right) electron-phonon coupling regime. It is remarked that the hole can be in one of the bandstates, represented by the dashed parabolas. For strong electron-phonon coupling, hole emission proceeds via a thermal barrier and is therefore temperature dependent, similar to hole capture in BTI. By contrast, for weak electron-phonon coupling, the parabola of the positive defect lies inside others and thus hole emission is dominated by a direct transitions without a thermal barrier. As a consequence, this transition is independent of the temperature, just as the gate current fluctuations.

the defect returns back to its neutral state 1. This switching behavior can explain the correlation seen in the drain and gate current noise mentioned above.

It is emphasized that the gate current fluctuations are actually temperature insensitive. At a first glance, this fact may contradict the above explanation since NMP transitions involve barriers, which must be thermally overcome (cf. Fig. 9). However, this is not the case for NMP transitions in the "weak electron-phonon coupling" regime (see Fig. 9). Such transitions were found to be the dominating NMP transition in TAT thereby explaining the temperature independent gate currents.

The above investigations were focused on single defects, whose impact on the gate leakage current must be studied in terms of reliability. It was learned so far that the defects start carrying a TAT current upon application of a gate bias. This behavior is reminiscent of stress-induced leakage current (SILC), which poses a problem to device reliability just as BTI and RTN. Therefore, SILC is likely caused by defects following the trapping kinetics of the four-state NMP model.

## Conclusions

The four-state NMP model can describe the charge capture and emission into and out of BTI defects and is consistent with a long list of criteria obtained from TDDS measurements and CET maps. It could also be demonstrated that those BTI defects are also responsible for RTN. Moreover, the four-state NMP model also gives an explanation for fluctuations in the gate current, thereby further corroborating the validity of this model. As such, this model provides a comprehensive description of oxide defects in reliability issues and unravels related reliability topics, such as SILC. As the model is determined by its defect parameters, understanding the nature of their distributions is of high importance.

## Acknowledgements

This work has received funding from the Austrian Science Fund (FWF) project n°23390-N24, the European Community's FP7 n°261868 (MORDRED), and the Intel Sponsored Research Project n° 2013111914.

## References

[1] V. Huard, *Proc.IRPS* (2010), pp. 33 –42.
[2] M. Kirton *et al.*, Adv.Phys. **38**, 367 (1989).
[3] T. Grasser *et al.*, IEEE Trans.Elect.Dev. **58**, 3652 (2011).
[4] K. Huang *et al.*, Proc.Roy.Soc. of London. Series A **204**, 406 (1950).
[5] A. Palma *et al.*, Phys.Rev.B **56**, 9565 (1997).
[6] T. Grasser *et al.*, *Proc.IEDM* (2011), pp. 27.4.1–27.4.4.
[7] T. Grasser *et al.*, *Proc.IRPS* (2013), pp. 2D.2.1–2D.2.7.
[8] T. Grasser *et al.*, *Proc.IRPS* (2012), pp. XT.8.1–XT.8.7.
[9] T. Grasser *et al.*, *Proc.IEDM* (2012), pp. 19.6.1–19.6.4.
[10] T. Grasser *et al.*, *Proc.IEDM* (2013), pp. 15.5.1–15.5.4.
[11] T. Grasser *et al.*, *Proc.IRPS* (2014), pp. 4A.5.1–4A.5.7.
[12] M. Toledano-Luque *et al.*, Microelectron.Eng. **88**, 1243 (2011).
[13] M. Waltl *et al.*, *Proc.IRPS* (2014), pp. XT18.1–XT18.5.
[14] C. Henry *et al.*, Phys.Rev.B **15**, 989 (1977).
[15] W. Goes *et al.*, *The Bias Temperature Instability: Experiment, Theory, and Modeling for Devices and Circuits* , edited by T. Grasser (Springer-Verlag, 2013), Chap. Advanced Modeling of Oxide Defects.
[16] A. Lelis *et al.*, IEEE Trans.Nucl.Sci. **41**, 1835 (1994).
[17] F. Schanovsky *et al.*, JCE **11**, 218 (2012).
[18] T. Grasser *et al.*, *Proc.IRPS* (2009), pp. 33–44.
[19] J. de Nijs *et al.*, Appl.Phys.Lett. **65**, 2428 (1994).
[20] P. Blöchl *et al.*, Phys.Rev.Lett. **83**, 372 (1999).
[21] J. Conley *et al.*, IEEE Trans.Nucl.Sci. **39**, 2186 (1992).
[22] T. Grasser, Microelectron.Reliab. **52**, 39 (2012).
[23] H. Reisinger *et al.*, *Proc.IRPS* (2010), pp. 7–15.
[24] T. Grasser, edited by T. Grasser (Springer NY, 2013), Chap. The Capture/Emission Time Map Approach to the Bias Temperature Instability.
[25] A. Alkauskas *et al.*, Phys.B Condens.Matter **401-402**, 546 (2007).
[26] Z.-Y. Lu *et al.*, Phys.Rev.Lett. **89**, 285505 (2002).
[27] P. Sushko *et al.*, J.Phys.-Condens.Matter **17**, S2115 (2005).
[28] K. Jeppson *et al.*, J.Appl.Phys. **48**, 2004 (1977).
[29] M. Toledano-Luque *et al.*, *Proc.IRPS* (2012).
[30] C.-Y. Chen *et al.*, *Proc.IRPS* (2011).
[31] B. Kaczer *et al.*, Microelectron.Eng. **109**, 123 (2013).
[32] X. Ji *et al.*, *IPRS* (2013), pp. XT.7.1–XT.7.5.
[33] O. Baumgartner *et al.*, *Proc.SISPAD* (2013).
[34] W. Goes *et al.*, *Proc.IPFA* (2013), pp. 51–56.
[35] W. Goes *et al.*, ECS Trans. **58**, 31 (2009).
[36] F. Jimenez-Molinos *et al.*, J.Appl.Phys. **90**, 3396 (2001).
[37] L. Vandelli *et al.*, *ESSDERC* (2010), pp. 388–391.
[38] L. Vandelli *et al.*, IEEE Trans.Elect.Dev. **58**, 2878 (2011).